

Magnetoresistance measurement of tailored Permalloy nanocontactsA. K. Patra,¹ A. von Bieren,^{1,2} S. Krzyk,¹ J. Rhensius,^{1,3} L. J. Heyderman,³ R. Hoffmann,⁴ and M. Kläui^{1,2,*}¹*Fachbereich Physik, Universität Konstanz, Universitätsstrasse 10, D-78457 Konstanz, Germany*²*Laboratory for Nanomagnetism and Spin Dynamics, Ecole Polytechnique Fédérale de Lausanne, CH-1015 Lausanne, Switzerland and SwissFEL, Paul Scherrer Institut, CH-5232 Villigen PSI, Switzerland*³*Laboratory for Micro- and Nanotechnology, Paul Scherrer Institut, CH-5232 Villigen PSI, Switzerland*⁴*Physikalisches Institut and DFG-Center for Functional Nanostructures, Karlsruhe Institute of Technology, Campus South, D-76128 Karlsruhe, Germany*

(Received 14 July 2010; revised manuscript received 5 October 2010; published 28 October 2010)

We study the evolution of the magnetoresistance (MR) in Permalloy nanocontacts prepared by controlled low-temperature UHV electromigration in nanoring segment structures with constrictions. The ring geometry allows for the controlled and reproducible positioning of a domain wall in the nanocontacts. We observe three different resistance levels, corresponding to distinct domain-wall positions. A change in the sign of the MR difference, between a domain wall at the constriction and a domain wall next to the constriction, occurs with decreasing constriction width. This is in line with our micromagnetic simulations, where the MR is calculated based on the anisotropic MR (AMR) effect.

DOI: [10.1103/PhysRevB.82.134447](https://doi.org/10.1103/PhysRevB.82.134447)

PACS number(s): 75.47.-m, 72.25.Ba, 73.63.Rt, 75.75.-c

I. INTRODUCTION

Domain walls in magnetic nanostructures have been intensively investigated due to their potential for applications in future devices, such as magnetic logic gates¹ and the race-track memory,² and due to exciting magnetotransport properties [quantized magnetoresistance (MR) effects], which are expected to occur for ultranarrow walls. The interaction between the spin-polarized current and such narrow domain walls leads to interesting physics such as large magnetoresistance effects and has gathered significant attention.³ The spin-polarized current can exert a torque on the localized spins of the domain wall and causes domain-wall motion in the direction of electron flow, which is called current-induced domain-wall motion.⁴ Reciprocally, noncollinear spin structures in the domain wall scatter the spin-polarized conduction electrons and this leads to domain-wall MR (DWMR).^{3,5} However, significant scattering of the conduction electrons due to the presence of a domain wall is expected only in the case of a narrow domain walls, where the spatial magnetization direction changes abruptly and therefore the conduction electrons are unable to adiabatically follow the local magnetization direction inside the domain wall.^{3,6} While intuitively one expects inhomogeneous magnetization in a domain wall to hinder the electron flow and cause an increase in the resistance, i.e., positive DWMR, there are theoretical predictions of positive^{6–9} as well as negative^{8–10} DWMR. Positive DWMR is explained considering mixing of the spin-up and spin-down channels due to the magnetization rotation within the domain wall.⁷ On the other hand, negative DWMR is ascribed to a weak localization effect, where the quantum contribution to the resistivity is reduced by the decoherence of the electron due to the presence of a domain wall.¹⁰ In addition DWMR of either sign is also predicted, taking into account the change in the electronic structure due to the rotating magnetization inside a domain wall.^{8,9}

For most realistic wall widths, the intrinsic contribution of the domain wall to the MR has been predicted to be small.

Therefore, it is difficult to discriminate the real DWMR response from other effects. Nevertheless, in MR measurements on highly anisotropic materials such as CoPt, FePt, and Co, a clear signature of the DWMR (mostly positive) is observed.^{6,11–17} This is possible because these materials exhibit narrow domain walls due to the high anisotropy, and the intrinsic domain-wall resistance R_{DW} has been predicted to scale with the inverse square of the domain-wall width d , i.e., $R_{DW} = 1/d^2$ (Refs. 3, 6, and 7). In contrast, the domain-wall contribution to the MR in soft magnetic materials such as Fe, polycrystalline Co, Ni, and Ni₈₀Fe₂₀ (Refs. 18–24) is often negative, which some have considered as an intrinsic DWMR of negative sign. However, the negative contribution of the domain wall to the MR is usually due to anisotropic MR (AMR), which depends on the angle θ between the direction of current flow and magnetization.²⁵ The resistance is higher (lower) when the current and magnetization are parallel/antiparallel (perpendicular) to each other and for bulk polycrystalline samples the AMR is proportional to $\cos^2 \theta$ (Ref. 26). Since the magnetic moments in a domain wall have magnetization components oriented perpendicularly to the current, the introduction of a domain wall to a single domain sample leads to a decrease in the resistance due to AMR.²⁵

Thus there is a clear need to discriminate between AMR and DWMR and in order to isolate the contribution from DWMR, the AMR needs to be ascertained independently especially for samples with narrow domain walls, which can be obtained by reducing the lateral dimensions of the sample. The samples have so far been produced mostly by electron-beam lithography, a technique that is limited to sample sizes down to 10–50 nm. To date, in particular, in soft magnetic materials there has been no systematic study on the MR in narrow domain walls, in nanowires with widths below sizes that can be achieved by lithography and where DWMR may become significant.

In this work, we report on the evolution of MR in tailored Permalloy (Py) (Ni₈₀Fe₂₀) nanocontacts. Due to the absence of any freestanding part of the magnetic layer and low mag-

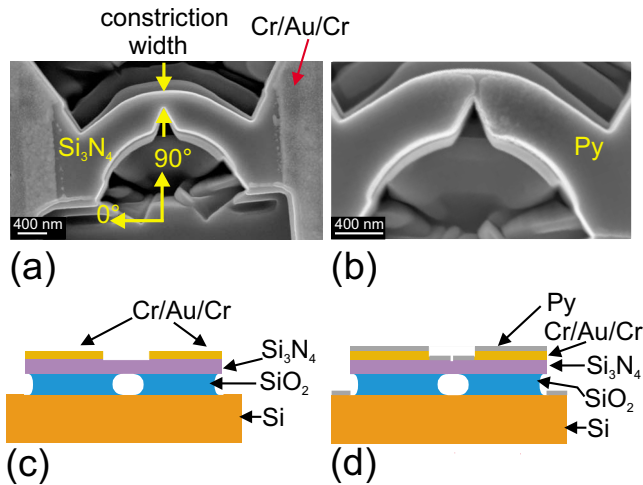


FIG. 1. (Color online) (a) Scanning electron microscope (SEM) image of a freestanding ring segment structure with a constriction at the center, prior to the deposition of Permalloy. The constriction width is indicated by two small vertical arrows and the in-plane field angles (ψ) for MR measurements are indicated by large arrows. (b) SEM image of an opened Permalloy nanocontact obtained after several electromigration cycles. A schematic of the cross-sectional view of the structure (c) prior to the writing of the ring segment by focused ion beam and (d) after the opening of the nanocontact is shown. The schematics (c) and (d) depict the situation of the SEM pictures shown in (a) and (b), respectively.

netostriction of the Py (Ref. 27), these nanocontacts are mostly mechanically stable and free of magnetostrictive effects at zero field. Constriction widths (CWs) varying from 220 nm to a few nanometers are obtained in a single nanocontact by controlled *in situ* electromigration in Permalloy nanoring segments with constrictions. This allows us to qualitatively and quantitatively study the MR behavior of the nanocontact as a function of constriction width. Due to the curvature, the ring geometry allows for the controlled and reproducible positioning of a domain wall in the sample²⁵ and a domain wall can be confined at the constriction.²⁸ Strikingly, our investigation down to contact sizes of a few nanometers suggests that in Py nanocontacts, the MR is dominated by AMR even for narrower constriction widths. We find that the difference in the MR signal between different domain-wall positions changes sign, due to the interplay between the current density and magnetization, as we reduce the constriction width. We reproduce this by micromagnetic simulations of the MR just taking into account the contribution due to AMR. Our investigations allow for the unambiguous determination of the domain-wall magnetoresistance and suggest that one has to consider the role of AMR more seriously.

II. EXPERIMENTAL

Permalloy nanocontacts were prepared using a combination of electron-beam lithography and focused ion-beam (FIB) techniques followed by dry and wet etching (see Fig. 1). First, Cr (5 nm)/Au (30 nm)/Cr (5 nm) pads were fabricated on Si_3N_4 (200 nm)/ SiO_2 (500 nm)/Si substrates by

electron-beam lithography and electron-beam evaporation. Using the top Cr layer as a mask, the samples were processed by reactive ion etching to remove the Si_3N_4 layer which is not covered by the Cr mask. After that, the samples were placed in an HF bath to remove the exposed SiO_2 layer and to obtain an undercut [Fig. 1(c)]. The realization of the undercut is essential to avoid any undesirable short circuit of the Py nanoring segment to the Py-covered Si substrate, arising from slightly oblique deposition of the Py layer at a small angle with respect to the surface normal. After the HF etching step, a 60° segment of a ring structure with a constriction at the center was written by FIB, which leads to a freestanding Si_3N_4 ring segment with a constriction [see Fig. 1(a)], on which the Py is deposited. In a final processing step, the metallic layers (Cr/Au/Cr) were removed from the ring segment using FIB. Due to the curvature, ring structures are an apt geometry for the controlled positioning of domain walls.²⁵ Moreover the detailed spin structures of such Py ring nanostructures are well established by transport measurements and imaging techniques.^{25,29–33} These results allow for an easy interpretation of the MR data obtained from the Py nanocontacts. Prior to the Py deposition, electrical contacts were made on Cr/Au/Cr contact pads by wire bonding. Then the samples were loaded into the ultrahigh vacuum chamber (base pressure of 5×10^{-10} mbar) and 12 nm of Py was deposited in a molecular-beam epitaxy chamber at room temperature. Magnetoresistance measurements (with a current $I < 100 \mu\text{A}$) were carried out at 77 K in a two-probe configuration with an in-plane magnetic field (± 100 mT).³⁴ The angle-dependent MR response of the nanocontact shows a $\cos^2 \theta$ dependence [see Fig. 2(a)], as expected for AMR in bulk samples. This suggests that the applied field strength is large enough to align the magnetization along the field directions. Furthermore, we are interested in the MR response measured at remanence for different magnetization configurations. To attain these configurations, a maximum field of 100 mT is sufficient. In order to tailor the constriction widths, electromigration cycles^{35,36} were performed on the samples at 77 K using the same electrical contacts used for MR measurements. Our electromigration process is based on the principle described in Ref. 36. A large current (~ 1 mA with the exact value depending on the state of the electromigration) is sent through the nanoring segment to heat the metallic layer locally. The increased temperature locally enhances diffusion. Electromigration effects cause a preferred direction of the diffusion such that the contact is narrowed locally. A computer-controlled process allows us to limit the temperature of the sample during electromigration such that local melting is prevented. Due to the geometry of the sample, the current density at the constriction is highest [see Fig. 4(a): a simulated current-density profile for a 90 nm constriction width]. Therefore, electromigration mostly takes place at that position and reduces the constriction width and thus increases the overall nanocontact resistance. Controlled electromigration was performed until the desired resistance was achieved.³⁶ After that, the MR was studied in different measurement modes. Then, the controlled electromigration process was continued until a larger resistance (and therefore smaller constriction width) was reached and the MR measurements were repeated. This procedure was repeated until

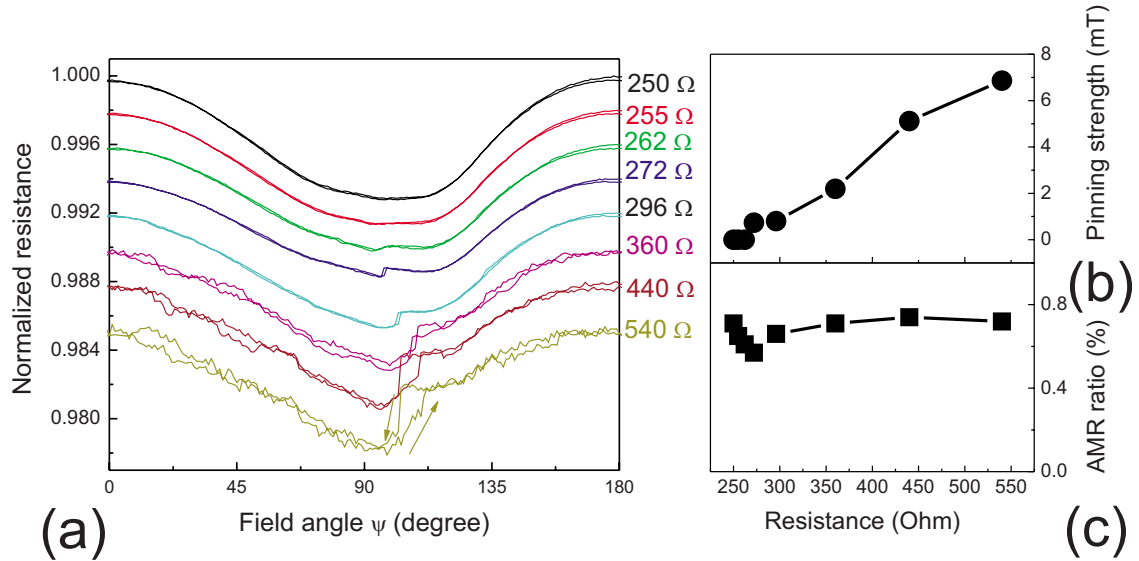


FIG. 2. (Color online) (a) Angular variation in the magnetoresistance curves for different resistance values, obtained by progressive electromigration of the nanocontact, measured at 77 K with a 42 mT in-plane field. The curves are offset along the y axis for clarity. (b) Pinning strength and (c) AMR ratio extracted from the MR curves [shown in Fig. 2(a)] as a function of the measured resistance.

the contact was finally opened completely so that no further electromigration could be carried out. The Py (12 nm thickness) ring segment structure had a constriction width of 220 nm (\approx half of the ring width) and a base resistance of 250 Ω before starting the electromigration. In Fig. 1, a scanning electron microscope (SEM) image of (a) a nanocontact prior to the Py deposition and electromigration and (b) an opened nanocontact obtained after significant electromigration are shown. A gap on the order of few tens of nanometers can be seen at the center [Fig. 1(b)], indicating that a localized and controlled electromigration at the constriction position has taken place. Unlike the nanocontacts fabricated using mechanical break junctions, these electromigrated Py nanocontacts are mostly mechanically stable because there is no free-standing part of the magnetic layer whose magnetoresistance is measured (the Py layer is supported by the 200 nm thick Si_3N_4 layer, which is a freestanding layer). Moreover, the magnetostriction constant of Py is low²⁷ and our key measurements are carried out at remanence in the absence of any applied field. Therefore, these nanocontacts are mostly magnetostriction free in addition to their mechanical stability and allow us to reduce the contribution of other spurious effects to the MR signal.

III. RESULTS AND DISCUSSION

For each chosen resistance value of the nanocontact, we first studied the AMR of the nanometer-sized sample by measuring the resistance when a field of constant amplitude (42 mT) is rotated [Fig. 2(a)]. The direction ψ along which the magnetic field was applied is indicated with arrows in Fig. 1(a). The normalized resistance as a function of field angle shows the typical $\cos^2 \theta$ ($\theta \approx \psi$ for sufficient magnetic field strength) expected for AMR in bulk samples.²⁶ A $\cos^2 \psi$ behavior is expected considering that the angle between the direction of current and local magnetization θ varies across

the ring segment due to its curvature: On one hand, the current flow follows the ring structure, i.e., the perimeter of the ring. On the other hand, the magnetization of the sample is aligned along the applied field direction.²⁵ However, the $\cos^2 \psi$ behavior is not as smooth as in the case of the bulk, which is ascribed to imperfections of the nanostructure geometry. Nevertheless, as expected, the resistance is larger for a magnetic field applied along 180° (or 0°), where the magnetization of most of the ring segment is roughly aligned parallel (or antiparallel) to the current direction and the resistance is lower for a field applied along 90° for which the magnetization and current are mostly perpendicular to each other. For intermediate angles, the resistance values lie between the two limiting values [$R(90^\circ) < R(\psi) < R(180^\circ)$]. A similar functional dependence of the resistance on the field angle is observed for all constriction widths reduced in successive electromigration cycles. For nanocontact resistances of $R_N \geq 272 \Omega$ additional features appear. Reproducible hysteretic resistance jumps close to the angles corresponding to the constriction location (90°) are observed. These jumps and the hysteresis are indications of the pinning and depinning of the spin structure at the constriction. For smaller constriction widths, larger jumps and a more pronounced hysteresis are observed. From the hysteresis one can estimate the pinning strength of the constriction for a given resistance. Here, the pinning strength is evaluated as $H \sin \Delta\psi$ with $\mu_0 H = 42$ mT, where $\Delta\psi$ is taken from the hysteresis of the MR curves [Fig. 2(a)]. The deduced pinning strength as a function of the sample resistance is depicted in Fig. 2(b). As expected, with increasing R_N , which corresponds to decreasing constriction width, the pinning strength increases and reaches in this measurement an effective necessary depinning field of 7 mT for $R_N = 540 \Omega$. Moreover, we can extract the AMR ratio [$\{(R_{\max} - R_{\min}) / R_{\max}\} \times 100$] from the MR curves shown in Fig. 2(a). The extracted AMR ratio as a function of the resistance is depicted in Fig. 2(c). The AMR

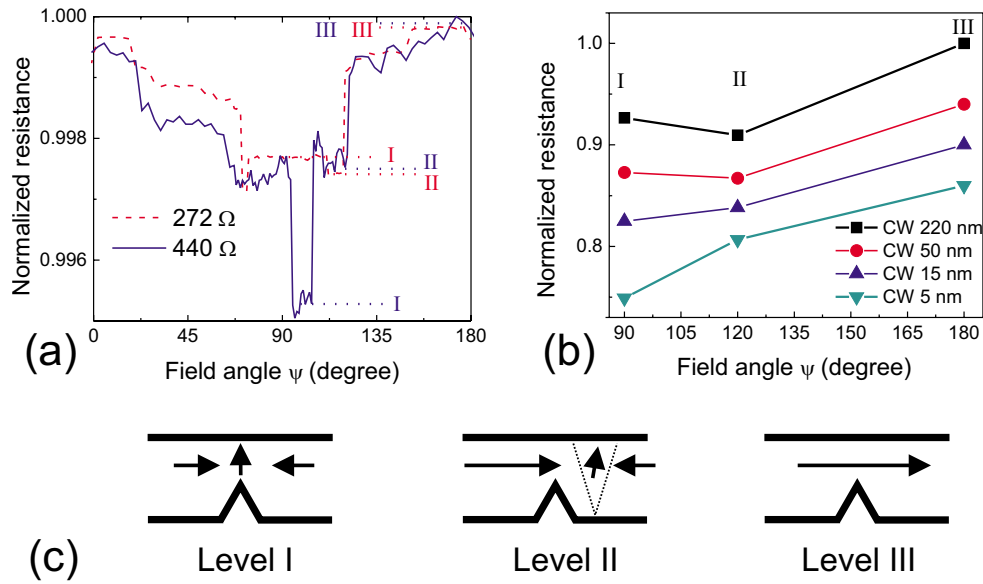


FIG. 3. (Color online) (a) Measured MR curves at remanence as a function of field angle [see the arrows in Fig. 1(a)] for two selected resistance values. An in-plane field of 42 mT was applied at a given angle and was relaxed to zero before carrying out the MR measurement for that particular angle. The constriction position corresponds to 90° [see Fig. 1(a)]. (b) Simulated MR values for different CWs. Lines in Fig. 3(b) are a guide to the eyes. (c) Schematic spin configurations for the presence of a domain wall at the different positions of the ring structure and the absence of a domain wall. I, II, and III denote three different resistance levels and correspond to the case of a domain wall at the constriction, a domain wall next to the constriction, and the absence of a domain wall, respectively.

ratio stays approximately constant for the whole resistance range investigated here. In addition, the maximum AMR ratio is just below 1%, which is in agreement with reports on Py (Refs. 23 and 27) with constriction widths down to a few nanometers. The observed MR value can thus be ascribed to a bulk AMR effect and is not due to ballistic AMR or tunneling AMR effects reported for nanocontact resistances in the $k\Omega$ to $M\Omega$ regime.^{27,37}

Next, for the same contact resistance, we measured the resistance values for a domain wall located at various positions, in particular, at the constriction position as well as next to the constriction. For this we employed the measurement scheme first used in Ref. 25, where we saturate the sample along a certain direction and relax the field to zero to measure the resistance for different positions of the domain wall. In this measurement a field of 42 mT was applied in order to saturate the sample. At remanence, after reducing the applied field to zero for a given angle, the minimization of magnetostatic energy and shape anisotropy of the ring leads to three different situations as sketched in Fig. 3(c): (I) *a domain wall can be situated at the constriction*, which is possible for fields applied along 90° , meaning that the field points in the direction of the constriction position or at angles close to this direction. In this situation the magnetization in the arms of the ring follow the perimeter of the ring and is aligned in opposite directions in the two arms with a domain wall at the center, i.e., at the constriction [Fig. 3(c), first sketch and Figs. 4(b) and 4(c) for simulated magnetization configuration]. (II) *A domain wall can be located in the ring but outside the constriction* [Fig. 3(c) second sketch]. (III) *Absence of domain walls in the ring*. This configuration is expected for fields applied at angles larger than 120° and for angles smaller than 60° , where the magnetization configuration fol-

lows exactly the perimeter of the ring without a domain wall [Fig. 3(c) third sketch]. Figure 3(a) shows the normalized resistance measured at remanence as a function of the field angle for two different overall nanocontact resistances ($R_N = 272 \Omega$ and 440Ω as examples) reached after different electromigration cycles. As expected, three different resistance levels (named I, II, and III) corresponding to the three scenarios described above are observed for both resistance values at the anticipated range of angles. The appearance of these levels can be understood in terms of AMR while taking into account the spin configuration of the three scenarios discussed above. The current in the ring always follows the perimeter of the ring and the current density is highest at the constriction [see Fig. 4(a)]. The resistance at $\psi > 120^\circ$ or $\psi < 60^\circ$ (level III) is largest because in this situation the current and magnetization are parallel to each other at all positions of the ring segment. Scenario I and II exhibit a domain wall where the magnetization direction inside the wall has a perpendicular component to the current direction. Therefore,

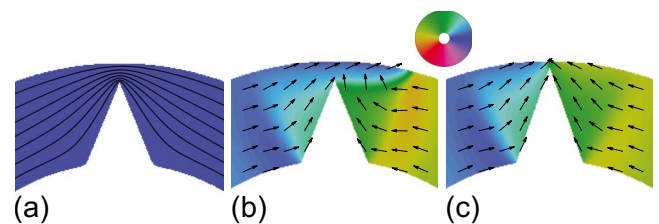


FIG. 4. (Color online) (a) A simulated current-density profile for a constriction width of 90 nm. (b) Simulated magnetization configuration for the case of a domain wall near the constriction for a constriction width 90 nm and (c) 30 nm. The magnetization direction is indicated by the color disk.

again due to the AMR, the resistance of the nanocontact with a domain wall is lower compared to the situation without a wall.

Surprisingly, we observe a sign change from positive to negative in the MR difference between level I and level II as the overall nanocontact resistance increases due to a decreasing constriction width. This suggests that the constriction width plays a key role in the MR properties of the nanocontacts. The absolute resistance values of level I and level II both depend on the magnitude of the current at the position of the domain wall and on the width of the domain wall since, as mentioned above, AMR is proportional to $j \cdot M \cos^2 \theta$, where j , M , and θ are current density, magnetization, and angle between the direction of current and local magnetization, respectively.³ The geometry of the ring segment including the constriction leads to a smaller domain-wall width for the wall residing in the constriction compared to the wall located in the arm of the ring because that reduces the exchange energy. On the one hand, the width of the domain wall and thus the area in which the resistance is lowered due to AMR is much smaller when the wall is located in the constriction compared to the situation where the wall is located in the ring segment. On the other hand, the current density at the constriction is higher, which means that the constriction dominates the voltage drop and thus the resistance of the nanocontact. Therefore, a reduction in the MR at the constriction due to the presence of the wall reduces the total resistance. The interplay of these two effects leads to the following observation: for a wide constriction—the resistance level I—domain wall at the constriction—is higher compared to level II—domain wall next to the constriction—and the difference between the level I and level II is positive. This behavior is indeed observed for $R_N=272 \Omega$ [dashed line in Fig. 3(a)]. For narrow constriction widths the resistance difference between the level I and level II is expected to be negative and we do observe such behavior for $R_N=440 \Omega$ [see Fig. 3(a) blue curve] where the constriction is expected to have a width of a few nanometers only. Such a difference in resistance (level I–level II), which is positive or negative, depending on the domain-wall width and the current density at the domain-wall position, can tempt one to attribute this to positive or negative intrinsic DWMR. We therefore evaluate the difference between level I and level II by assuming a magnetoresistance based on AMR and using micromagnetic simulations to obtain the magnetization configuration.

We simulate the spin configuration and the current-density profile using numerical methods for the ring structure with different constriction widths as a function of field angle. We employ the LLG micromagnetic simulator³⁸ and calculate the AMR using the procedure described in Ref. 25. For the simulation, the starting constriction width (i.e., 220 nm) was the one obtained from the SEM picture taken prior to the measurement [see Fig. 1(a)]. We use $M_s=800 \times 10^3 \text{ A/m}$, $A=10.5 \times 10^{-12} \text{ J/m}$, $K_1=1.0 \times 10^2 \text{ J/m}^3$, a constant thickness of 12 nm, and a cell size of 5 nm. To reduce the computation time, a damping parameter $\alpha=1$ was used which leads to the same final spin configuration as a small (realistically, $\alpha=0.01$) damping parameter. In the case of constriction widths of less than 5 nm, the center cell at the con-

striction was replaced by a smaller (down to 1 nm) cell size.³⁹ A variable cell size approach was used for the current-density simulations, too. A simulated current-density profile for a constriction width of 90 nm and the magnetization configuration for the case of a domain wall near the constriction for two constriction widths (90 and 30 nm) are shown in Fig. 4. A change in the resistivity, which may occur right at the constriction, is taken into consideration while calculating the AMR response of the nanocontacts. For a given constriction width, the corresponding resistance is calculated using Wexler's formula,⁴⁰ which is valid in the diffusive and ballistic regime of conduction,

$$R_w = \frac{4}{3\pi} \frac{\rho l}{r^2} + \gamma \frac{\rho}{2r},$$

where ρ is the resistivity, l is the electron mean-free path, r is the contact radius, and γ is defined as

$$\gamma(r/l) = \frac{1 + 0.83(l/r)}{1 + 1.33(l/r)}.$$

We use $l=1 \text{ nm}$ (Ref. 41) and $\rho=40 \mu\Omega \text{ cm}$.⁴² Then, from the calculated resistance we estimate the effective resistivity which also includes quantum effects for atomic size constrictions. As expected, an increase in the effective resistivity with decreasing constriction width is observed. The effective resistivity for 1 nm constriction width is more than twice the bulk resistivity ($\rho=40 \mu\Omega \text{ cm}$). In order to thoroughly check the influence of quantum effects, in particular, within the volume given by a radius of the mean-free path of Permalloy taken around the constriction, we additionally performed simulations with a smaller cell size and a locally varying resistivity. An influence was only observed for the smallest constriction sizes but remained below 2% and therefore does not change the overall interpretation of the simulations. The normalized resistances obtained from the simulation are shown in Fig. 3(b). Similar to the experiment, three resistance levels are observed and also the resistance for the case of no domain wall [level III in Fig. 3(b)] is higher compared to the case of a domain wall in the structure [levels I and II in Fig. 3(b)]. Moreover, a sign change in the difference between the resistances of levels I and II is also observed for smaller constriction widths in agreement with our experimental results.

To evaluate the resistance difference between levels I and II and, in particular, the observed sign change, the difference of the normalized resistance (normalized to the maximum AMR value for that particular measured resistance or simulated constriction width) between levels I and II (ΔR_{I-II}) is plotted as a function of the resistance of the nanocontact in Fig. 5(a). The ΔR_{I-II} changes its sign from positive to negative when the nanocontact resistance increases beyond 340 Ω . Moreover, the magnitude of the ΔR_{I-II} increases with further increasing the resistance, i.e., for smaller constriction widths. This indicates that the constriction plays a dominant role in the transport behavior. The sign change in the ΔR_{I-II} can be understood from the AMR, as already discussed. This

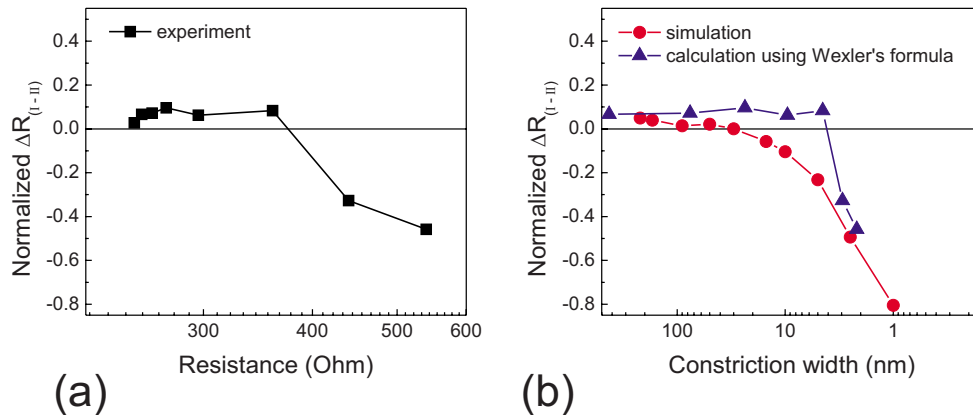


FIG. 5. (Color online) (a) Resistance difference between level I [domain wall at the constriction, see Fig. 3(a)] and level II [domain wall next to the constriction, see Fig. 3(a)] normalized by the AMR $[(R_{\max} - R_{\min})/R_{\max}]$ measured with 42 mT, ΔR_{I-II} , obtained from measurement as a function of resistance of the nanocontact. (b) The normalized ΔR_{I-II} , as a function of constriction width (filled circles) obtained from the simulation and from the experiment, calculated (filled triangles) using Wexler's formula with a electron mean free path $l=1$ nm and resistivity $\rho=40 \mu\Omega$ cm from the measured resistance values.

trend is also visible in the simulated data shown in Fig. 5(b) (filled circles), where the simulated ΔR_{I-II} is plotted as a function of the constriction width.

In order to compare the measured and simulated data more quantitatively, a suitable conversion of the experimentally measured resistance of the nanocontact to the constriction width is necessary, because in the experiment we measure the resistance, whereas in the simulation, different constriction widths are set. Therefore, to treat the measured and simulated data on equal footing, we calculate the constriction width for the measured resistance values using Wexler's formula⁴⁰ with an electron mean-free path $l=1$ nm (Ref. 41) and resistivity $\rho=40 \mu\Omega$ cm.⁴² The result is depicted in Fig. 5(b) (filled triangles) together with the simulated data in Fig. 5(b) (filled circles). Wexler's formula⁴⁰ considers a circular cross section (thickness=diameter=constriction width). However, SEM images taken before the electromigration show that a circular cross section is clearly not realized at the start of the process. At the start of the electromigration the constriction is much better described by a constriction width with constant film thickness where the width is reduced by successive electromigration. For the data shown in Fig. 5(b) we therefore deduced from the experimental data an effective constriction radius using Wexler's formula.⁴⁰ From this effective radius we calculated the constriction width that provides the same cross-sectional area as a circular cross section. On the other hand, for small constriction widths the constriction cross section might be of circular shape. For constriction widths below 12 nm (which is the thickness of the Py layer), we have therefore assumed a circular cross-section of the constriction. Moreover, the resistance of the leads is not included in Wexler's formula. We therefore included a base resistance of 250 Ω , which corresponds to our first resistance measurement taken before the start of electromigration.

Given this conversion of the nanocontact resistance to constriction width, we now compare the measured and simulated data [Fig. 5(b)]. As one can see, the constriction widths [filled triangles in Fig. 5(b)] calculated from the measured

resistance values using Wexler's formula agree qualitatively with the simulated constriction widths [filled circles in Fig. 5(b)]. However, a quantitative agreement is not observed. This,

on the one hand suggests, that Wexler's formula might not be fully applicable to our case. Here one has to consider that Wexler's formula is a simplified approach to calculate the resistance of a sample as a function of the contact cross section assuming that two big reservoirs are connected via a point contact.⁴⁰ This might not be the case in our nanocontact geometry, as the nanocontacts often form a chain of atoms and thus do not resemble the situation of Wexler's geometry. On the other hand, the discrepancy could arise from the fact that our simulated magnetization structure may not fully reproduce the real one at the constriction, in particular, for small constriction widths. Surface morphology and magnetocrystalline anisotropy, in particular, in view of possible residual few layer surface contamination of the sample are also not taken into account in the simulation. In addition to that, the MR is calculated using the bulk AMR magnitude. However, apart from the AMR, additional responses from other intrinsic effects, namely, the domain-wall magnetoresistance, which might be small and often buried under the AMR, cannot be ruled out. The domain-wall resistance is predicted to scale with $1/d^2$, with d being the domain-wall width so that for ultranarrow domain walls with ballistic transport this might become sizeable. For our case of low resistances of the Permalloy nanocontacts with diffusive transport, we do not observe any clear signature of the domain-wall resistance, which means that if there is such an effect, it is significantly smaller than our observed AMR effect. Although our simulated MR values based on the bulk AMR effect do not agree quantitatively with our measured curves, we find that a sign change in ΔR_{I-II} can be reproduced considering pure AMR as the source of the MR in the nanocontacts and a qualitative agreement between experiment and calculation is reached. This means that the AMR gives a dominant contribution to the MR signal of the electromigrated Permalloy nanocontacts. These findings allow

for an identification of the intrinsic signature of the domain-wall magnetoresistance when comparing experimental with calculated data.

IV. CONCLUSIONS

In conclusion, we have measured the MR curves as a function of constriction width for Py nanocontacts obtained by progressive electromigration. These nanocontacts are mechanically stable and largely free of magnetostriction. A domain wall is reproducibly and controllably placed in the nanocontact and its effect on the MR properties is discussed. Our low-temperature MR measurements are in agreement with the micromagnetic simulation obtained by numerical calculations based on the bulk AMR effect and reveal the existence of three different resistance levels. These levels, depending on the position of the domain wall in the nanocontact and its internal spin structure, are accessible at remanence for fields applied at different angles. The dominant contribution of the constriction to the MR of the nanocontacts is clearly visible. For smaller constriction widths a sign change in the MR difference between the case of a domain wall at the constriction and the case of a domain wall next to the constriction is found and can be qualitatively explained

by the AMR effect. However, we do not observe any intrinsic measurable signature of DWMR and/or ballistic magnetoresistance, whose effect might be small and buried under the AMR effect. The measured AMR ratios of these nanocontacts do not exceed 1% and the MR curves are dominated by the AMR effect even for the nanocontacts with a constriction size of a few nanometers. This study reveals that AMR plays a significant role and dominates the MR response of the nanocontacts made of soft magnetic Permalloy. Therefore, one has to take into account this AMR response carefully when trying to determine the intrinsic signature of domain-wall magnetoresistance.

ACKNOWLEDGMENTS

This work was supported financially by the German Science Foundation (DFG) (SFB 767, KL 1811), the Swiss National Science Foundation, the ERC (Starting Independent Researcher under Grants No. ERC 2007-Stg 208162 and No. 2010-Stg 239838), the EU (RTN Spinswitch, Grant No. MRTN CT-2006-035327), the Samsung Advanced Institute of Technology, and the Kompetenznetz “Funktionelle Nanostrukturen” of the Landesstiftung Baden Württemberg. We thank C. A. F. Vaz for useful discussions.

*Corresponding author; mathias.klaeui@epfl.ch

- ¹D. A. Allwood, G. Xiong, C. C. Faulkner, D. Atkinson, D. Petit, and R. P. Cowburn, *Science* **309**, 1688 (2005).
- ²S. S. P. Parkin, M. Hayashi, and L. Thomas, *Science* **320**, 190 (2008).
- ³C. H. Marrows, *Adv. Phys.* **54**, 585 (2005).
- ⁴L. Berger, *J. Appl. Phys.* **55**, 1954 (1984).
- ⁵A. D. Kent, J. Yu, U. Rüdiger, and S. S. P. Parkin, *J. Phys.: Condens. Matter* **13**, R461 (2001).
- ⁶M. Viret, D. Vignoles, D. Cole, J. M. D. Coey, W. Allen, D. S. Daniel, and J. F. Gregg, *Phys. Rev. B* **53**, 8464 (1996).
- ⁷P. M. Levy and S. Zhang, *Phys. Rev. Lett.* **79**, 5110 (1997).
- ⁸R. P. van Gorkom, A. Brataas, and G. E. W. Bauer, *Phys. Rev. Lett.* **83**, 4401 (1999).
- ⁹C. Wickles and W. Belzig, *Phys. Rev. B* **80**, 104435 (2009).
- ¹⁰G. Tatara and H. Fukuyama, *Phys. Rev. Lett.* **78**, 3773 (1997).
- ¹¹J. F. Gregg, W. Allen, K. Ounadjela, M. Viret, M. Hehn, S. M. Thompson, and J. M. D. Coey, *Phys. Rev. Lett.* **77**, 1580 (1996).
- ¹²U. Ebels, A. Radulescu, Y. Henry, L. Piraux, and K. Ounadjela, *Phys. Rev. Lett.* **84**, 983 (2000).
- ¹³D. Ravelosona, A. Cebollada, F. Briones, C. Diaz-Paniagua, M. A. Hidalgo, and F. Batallan, *Phys. Rev. B* **59**, 4322 (1999).
- ¹⁴M. Viret, Y. Samson, P. Warin, A. Marty, F. Ott, E. Sondergard, O. Klein, and C. Fermon, *Phys. Rev. Lett.* **85**, 3962 (2000).
- ¹⁵R. Danneau, P. Warin, J. P. Attane, I. Petej, C. Beigne, C. Fermon, O. Klein, A. Marty, F. Ott, Y. Samson, and M. Viret, *Phys. Rev. Lett.* **88**, 157201 (2002).
- ¹⁶C. Hassel, M. Brands, F. Y. Lo, A. D. Wieck, and G. Dumpich, *Phys. Rev. Lett.* **97**, 226805 (2006).
- ¹⁷A. Aziz, S. J. Bending, H. G. Roberts, S. Crampin, P. J. Heard, and C. H. Marrows, *Phys. Rev. Lett.* **97**, 206602 (2006).
- ¹⁸U. Ruediger, J. Yu, S. Zhang, A. D. Kent, and S. S. P. Parkin, *Phys. Rev. Lett.* **80**, 5639 (1998).
- ¹⁹K. Hong and N. Giordano, *J. Phys.: Condens. Matter* **10**, L401 (1998).
- ²⁰T. Taniyama, I. Nakatani, T. Namikawa, and Y. Yamazaki, *Phys. Rev. Lett.* **82**, 2780 (1999).
- ²¹Y. Otani, S. G. Kim, K. Fukamichi, O. Kitakami, and Y. Shimada, *IEEE Trans. Magn.* **34**, 1096 (1998).
- ²²U. Rüdiger, J. Yu, L. Thomas, S. S. P. Parkin, and A. D. Kent, *Phys. Rev. B* **59**, 11914 (1999).
- ²³K. Miyake, K. Shigeto, K. Mibu, T. Shinjo, and T. Ono, *J. Appl. Phys.* **91**, 3468 (2002).
- ²⁴N. Giordano and B. Çetin, *Phys. Status Solidi B* **241**, 2404 (2004).
- ²⁵M. Kläui, C. A. F. Vaz, J. Rothman, J. A. C. Bland, W. Wernsdorfer, G. Faini, and E. Cambril, *Phys. Rev. Lett.* **90**, 097202 (2003).
- ²⁶T. R. McGuire and R. I. Potter, *IEEE Trans. Magn.* **11**, 1018 (1975).
- ²⁷K. I. Bolotin, F. Kuemmeth, A. N. Pasupathy, and D. C. Ralph, *Nano Lett.* **6**, 123 (2006); K. I. Bolotin, F. Kuemmeth, and D. C. Ralph, *Phys. Rev. Lett.* **97**, 127202 (2006).
- ²⁸P. Bruno, *Phys. Rev. Lett.* **83**, 2425 (1999).
- ²⁹M. Kläui, H. Ehrke, U. Rüdiger, T. Kasama, R. E. Dunin-Borkowski, D. Backes, L. J. Heyderman, C. A. F. Vaz, J. A. C. Bland, G. Faini, E. Cambril, and W. Wernsdorfer, *Appl. Phys. Lett.* **87**, 102509 (2005).
- ³⁰M. Laufenberg, D. Backes, W. Bührer, D. Bedau, M. Kläui, U. Rüdiger, C. A. F. Vaz, J. A. C. Bland, L. J. Heyderman, F. Nolting, S. Cherifi, A. Locatelli, R. Belkhou, S. Heun, and E.

- Bauer, *Appl. Phys. Lett.* **88**, 052507 (2006).
- ³¹D. Backes, C. Schieback, M. Kläui, F. Junginger, H. Ehrke, P. Nielaba, U. Rüdiger, L. J. Heyderman, C. S. Chen, T. Kasama, R. E. Dunin-Borkowski, C. A. F. Vaz, and J. A. C. Bland, *Appl. Phys. Lett.* **91**, 112502 (2007).
- ³²D. Bedau, M. Kläui, U. Rüdiger, C. A. F. Vaz, J. A. C. Bland, G. Faini, L. Vila, and W. Wernsdorfer, *J. Appl. Phys.* **101**, 09F509 (2007).
- ³³J. Rhensius, L. Heyne, D. Backes, S. Krzyk, L. J. Heyderman, L. Joly, F. Nolting, and M. Kläui, *Phys. Rev. Lett.* **104**, 067201 (2010).
- ³⁴S. Krzyk, A. Schmidfeld, M. Kläui, and U. Rüdiger, *New J. Phys.* **12**, 013001 (2010).
- ³⁵H. Park, A. K. L. Lim, A. Paul Alivisatos, J. Park, and P. L. McEuen, *Appl. Phys. Lett.* **75**, 301 (1999).
- ³⁶R. Hoffmann, D. Weissenberger, J. Hawecker, and D. Stöffler, *Appl. Phys. Lett.* **93**, 043118 (2008).
- ³⁷M. Viret, M. Gabureac, F. Ott, C. Fermon, C. Barreateau, G. Autes, and R. Guirado-Lopez, *Eur. Phys. J. B* **51**, 1 (2006).
- ³⁸M. R. Scheinfein, LLG Micromagnetics Simulator, <http://llgmicro.home.mindspring.com>
- ³⁹For cell sizes smaller than 5 nm, the center cell was replaced by smaller cells. The distribution of the current and the magnetization directions as well as magnitude were mapped from the 5 nm cell size with appropriate numbers of neighbor cells.
- ⁴⁰W. Wexler, *Proc. Phys. Soc. London* **89**, 927 (1966).
- ⁴¹D. Y. Petrovykh, K. N. Altmann, H. Höchst, M. Laubscher, S. Maat, G. J. Mankey, and F. J. Himpsel, *Appl. Phys. Lett.* **73**, 3459 (1998).
- ⁴²L. K. Bogart and D. Atkinson, *Appl. Phys. Lett.* **94**, 042511 (2009).